

Co and Cu complexes with 2-acetylpyridine-4-hydroxy phenylacetyl acylhydrazone: Synthesis, crystal structures, CT-DNA/BSA binding behaviors, antibacterial activities and molecular docking studies

Jie Yang, Xiang-rong Liu*, Ming-kun Yu, Wen-bo Yang, Zai-wen Yang, Shun-sheng Zhao

College of Chemistry and Chemical Engineering, Xi'an University of Science and Technology, Xi'an 710054, China

ARTICLE INFO

Article history:

Received 22 January 2020

Accepted 25 May 2020

Available online 1 June 2020

Keywords:

Complex

Acylhydrazone

Crystal structure

DNA/BSA binding

Antibacterial activities

ABSTRACT

Two mononuclear complexes $[\text{Co}(\text{HL})\text{L}]\text{NO}_3$ (**1**) and $[\text{Cu}(\text{HL})_2](\text{NO}_3)_2$ (**2**) were synthesized from the reaction of 2-acetylpyridine-4-hydroxy phenylacetyl acylhydrazone (**HL**) with copper/cobalt nitrate hydrate. The single-crystal XRD results revealed the central Co and Cu ions in two complexes are both six-coordinated showing a distorted octahedral geometry. Thermal stabilities of **1**, **2** and **HL** were explored by thermogravimetry (TG) and the apparent activation energy (E_a) followed the order $2 > 1 > \text{HL}$. The interactions of **1**, **2**, **HL** with calf thymus DNA (CT-DNA) and bovine serum albumin (BSA) were investigated through UV-Vis absorption spectroscopy, fluorescence spectroscopy, microcalorimetry and molecular docking approach. From UV-Vis absorption spectroscopy and fluorescence spectroscopy results, it is shown that **1**, **2** and **HL** can bind with CT-DNA by intercalation mode and quench the fluorescence of BSA through static process. The binding constants K_{b} of three compounds toward CT-DNA/BSA followed the order: $1 > 2 > \text{HL}$. Thermogenic curves of three compounds interacting with CT-DNA and BSA were measured by microcalorimetry. The calculated enthalpies, entropies and Gibbs' free energy change ($\Delta H > 0$, $\Delta S > 0$, $\Delta G < 0$) indicated that all the interaction processes were endothermic and spontaneous. Molecular docking results further validated the intercalation binding mode of **1**, **2** and **HL** with CT-DNA and the fluorescence quenching of tryptophan in BSA in presence of three compounds. It also demonstrated that hydroxyl, benzene ring, pyridine ring, and carbonyl group of **1**, **2**, **HL** are the most favorable binding site in DNA/BSA interaction. The antimicrobial activities of **HL**, **1** and **2** against *Staphylococcus aureus* (*S. aureus*) and *Bacillus subtilis* (*B. subtilis*) were determined presenting that **1** and **HL** can inhibit the growth of *S. aureus* and *B. subtilis*, separately. Cellular uptakes of **1** and **2** into *S. aureus* and *B. subtilis* showed the amount of Co accumulation in *S. aureus* is bigger than that of Cu.

© 2020 Elsevier Ltd. All rights reserved.

1. Introduction

Acylhydrazones as a special kind of Schiff base have been widely investigated because their structures are similar to that of natural biological substances [1]. The C=N and N=N linkages in the acylhydrazone molecules play an essential role in the design and construction of promising bioactive agents [2–4]. As reported in many literature, acylhydrazones display various biological activities such as antithrombotic [5], antimicrobial [6], antitubercular [7], antimalarial [8], anticancer [9] and antioxidant [10] activities.

Moreover, acylhydrazones exhibit strong coordination abilities and flexible coordination modes due to the N, O donor atoms. It has also been found that acylhydrazones containing pyridine ring

are easier to coordinate because of the additional N donor atom. Many acylhydrazone complexes were synthesized and among which, much attention has been paid to Co and Cu complexes [11–15]. Cobalt and copper are indispensable trace elements in the human body. Co^{2+} could involve in the synthesis of vitamin B12 in vivo, which indirectly regulates the synthesis of DNA [16] while Cu^{2+} plays a vital role in enzymatic reactions [17–20]. When Co^{2+} or Cu^{2+} ion coordinates with organic ligand, the polarity of Co or Cu complex would be deduced because π -electron is delocalized over the chelate ring and the donor groups also partially share positive charge of the metal ion. And the reduction in polarity enhances the lipophilicity of the complex which consequently makes the permeation of complex through the lipid layer of organism more efficient [21,22].

Besides, DNA is the primary target for many kinds of drugs [23–28] and it plays an important role in gene regulation during

* Corresponding author.

E-mail address: liuxiangrongxk@163.com (X.-r. Liu).

the life process. Metal complexes could bind to DNA through electrostatic effect, groove binding or intercalation [29]. Serum albumins are significant biological macromolecules which can reversibly bind to drug molecules and transport them to target tissues and organs [30]. Compared with normal cells, tumor tissue cells have high vascular densities, large gaps between endothelial cells and abnormal lymphatic drainage. These abnormal features lead to the enhanced permeability and retention (EPR) effect of tumor tissue cells. Because of the EPR effect, complex-albumin adduct can easily accumulate in tumor tissue cells to meet their high energy needs for proliferation rather than normal cells [31,32]. Thus, serum albumins greatly influence the distribution and absorption of drugs [33]. Therefore, investigation on the interactions between the compound and DNA/serum albumins could ascertain the mechanism of drug effect and be beneficial in the design of new chemotherapy metal-based drugs [34].

In this work, a new acylhydrazone ligand containing pyridine ring (**HL**) and its Co(II) (**1**), Cu(II) (**2**) complexes were synthesized and their single crystals were obtained as well. The ligand and the complexes were characterized by elemental analyses, single-crystal X-ray diffraction, FT-IR and TG-DTG. The binding abilities of **HL**, **1** and **2** with calf thymus DNA (CT-DNA) were studied by UV-Vis spectroscopy. And the interactions of **HL**, **1** and **2** with bovine serum albumin (BSA) were explored by fluorescence spectroscopy. The interaction enthalpies and interaction time of **HL**, **1** and **2** with CT-DNA/BSA were determined by microcalorimetry. Moreover, in order to identify binding locations and mechanisms, the molecular docking of the three compounds with DNA/BSA were performed on Autodock 4.0 software. *Staphylococcus aureus* and *Bacillus subtilis* were used to evaluate the antibacterial activities of all compounds.

2. Experimental

2.1. Chemicals and methods

All chemicals are commercially available for analytical grade and used without further purification. Elemental analyses (C, H and N) for the compounds were carried out on a P.E. 2400-II instrument. Infrared spectra were obtained on a Bruker Tensor-II Fourier infrared spectrometer. The crystal structures of compounds were performed with graphite monochromator Mo-K α radiation ($\lambda = 0.71073 \text{ \AA}$) on a Bruker Smart Apex II CCD diffractometer and the data were collected by the $\omega/2\theta$ scan technique at 296(2) K. The crystal structures were solved by direct methods and fined by full-matrix least-squares on F^2 with the SHELXL program. Thermogravimetric analysis was carried out by the Mettler Toledo TGA analyzer. UV-Vis spectra were used to study the interaction between compounds and CT-DNA on TU-1900 spectrophotometer. BSA binding abilities of compounds were monitored by P. E. Fluorescence spectrometer LS55 ($\lambda_{\text{ex}} = 280 \text{ nm}$). Interaction enthalpies of compounds with CT-DNA/BSA were measured by C80 microcalorimeter. Antibacterial evaluations of compounds were determined by Mueller-Hilton agar media. The cellular uptake amounts of cobalt/copper complexes were measured by using NexION 350D ICP-MS.

2.2. Synthesis of compounds

2.2.1. Synthesis of 4-hydroxy phenylacetyl hydrazide

An alcoholic solution (5 mL) of methyl 4-hydroxyphenylacetate (1.6617 g, 10 mmol) was added to 80% hydrazine hydrate (8 mL) under continuous stirring. The mixture was heated at 80 °C and refluxed for 2–3 h. Then resultant solutions were filtered and stood for 3 d at room temperature to give the colorless crystals.

2.2.2. Synthesis of **HL** (2-acetylpyridine-4-hydroxy phenylacetyl acylhydrazone)

2-acetylpyridine-4-hydroxy phenylacetyl acylhydrazone was synthesized by the reaction of 4-hydroxy phenylacetyl hydrazine (0.0498 g, 0.3 mmol) and 2-acetylpyridine (33.6 μL , 0.3 mmol) in methanol (15 mL). And 2–3 drops acetic acid were added into the mixture as the catalyst. The mixture solution was refluxed and stirred for 3 h under 65 °C. Then the resultant solution was filtered and stood for 3 d at room temperature. The colorless single crystals were obtained. Yield: 72.46%. M.p.: 181–182 °C. Anal. Calc. for $\text{C}_{15}\text{H}_{15}\text{N}_3\text{O}_2$ (%) **HL**: C, 66.90; H, 5.61; N, 15.60. found: C, 67.15; H, 5.41; N, 15.13. IR (KBr, cm^{-1}): ($\nu_{\text{N-H}}$) 3256, ($\nu_{\text{C=O}}$) 1625, ($\nu_{\text{C=N}}$) 1596.

2.2.3. Synthesis of **1** ($[\text{Co}(\text{HL})\text{L}]\text{NO}_3$)

1 was prepared by stirring a mixture solution of **HL** (0.0538 g, 0.4 mmol), 5–10 drops pyridine and cobaltous nitrate hexahydrate (0.0290 g, 0.2 mmol) in ethanol (15 mL) for 4 h under 80 °C. The resultant solution was filtered and stood for 3 d at room temperature. The dull-red single crystals were obtained. Yield: 68.36%. M. p.: 242–244 °C. Anal. Calc. for $\text{C}_{30}\text{H}_{31}\text{CoN}_7\text{O}_7$ (%) **1**: C, 54.67; H, 4.43; N, 14.88. found: C, 54.28; H, 4.72; N, 14.26. IR (KBr, cm^{-1}): ($\nu_{\text{N-O}}$) 1376, ($\nu_{\text{N-H}}$) 3240, ($\nu_{\text{C=O}}$) 1608, ($\nu_{\text{C=N}}$) 1502, ($\nu_{\text{Co-O}}$) 538, ($\nu_{\text{Co-N}}$) 774 [35].

2.2.4. Synthesis of **2** ($[\text{Cu}(\text{HL})_2]\text{NO}_3$)

2 was prepared by stirring a mixture solution of **HL** (0.0538 g, 0.4 mmol) and cupric nitrate trihydrate (0.0242 g, 0.2 mmol) in methanol (15 mL) for 4 h under 65 °C. The resultant solution was filtered and stood for 3 d at room temperature. The green single crystals were obtained. Yield: 69.28%. M.p.: 204–205 °C. Anal. Calc. for $\text{C}_{30}\text{H}_{30}\text{CuN}_8\text{O}_{10}$ (%) **2**: C, 49.58; H, 4.16; N, 15.43. Found: C, 50.22; H, 3.72; N, 15.11. IR (KBr, cm^{-1}): ($\nu_{\text{N-O}}$) 1380, ($\nu_{\text{N-H}}$) 3247, ($\nu_{\text{C=O}}$) 1605, ($\nu_{\text{C=N}}$) 1585, ($\nu_{\text{Cu-O}}$) 535, ($\nu_{\text{Cu-N}}$) 634. The synthetic routes of **HL**, **1** and **2** are shown in Scheme 1.

2.3. Thermogravimetric experiments of **HL**, **1** and **2**

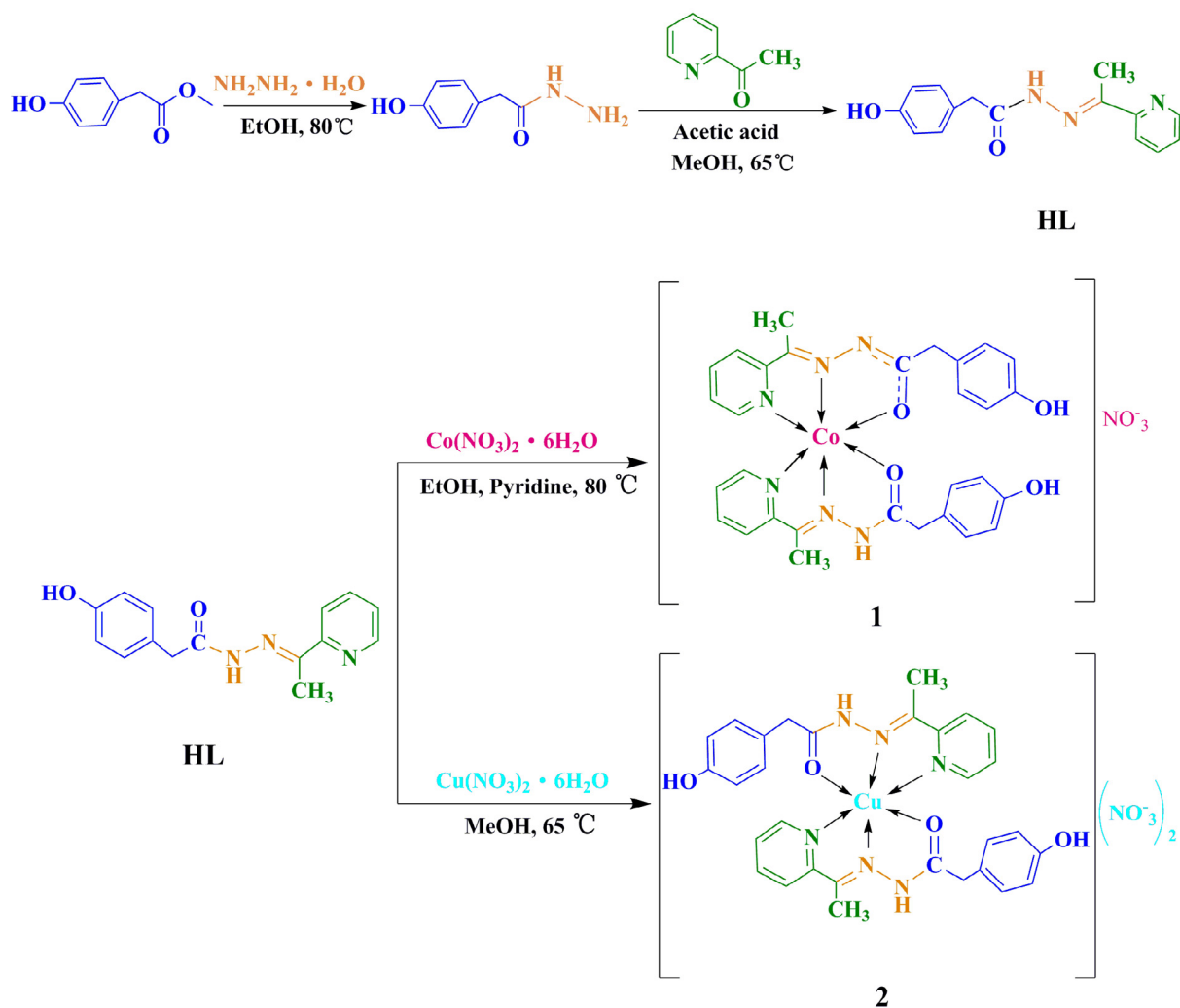
The TG curves of test compounds were obtained in N_2 atmosphere within the temperature range of room temperature to 800 °C. And the heating rates were set as 5, 10 and 15 °C $\cdot\text{min}^{-1}$.

2.4. CT-DNA-binding studied by UV-vis spectroscopy

The CT-DNA solution ($2.88 \times 10^{-4} \text{ M}$) was prepared by dissolving CT-DNA in Tris-HCl buffer solution (0.01 M, pH = 7.9). And the UV-Vis spectra of CT-DNA solution showed bands at 260 nm and 280 nm with a 1.8:1 ratio suggesting that the CT-DNA is free from protein. Test compounds were dissolved in mixed solution of DMSO and Tris-HCl (5:95, V/V) with concentration of $1 \times 10^{-4} \text{ M}$. CT-DNA solution (50 μL for each time) was dropped into the solutions of test compounds (3 mL) and reference solution (Tris-HCl-DMSO buffer solution). After each addition of CT-DNA, the UV-Vis spectra were recorded in the range of 250–500 nm under 28 °C.

2.5. BSA-binding studied by fluorescence spectroscopy

BSA solution ($1 \times 10^{-7} \text{ M}$) was prepared by dissolving BSA in Tris-HCl-NaCl buffer solution (0.01 M, pH = 7.2). The solutions of test compounds ($1 \times 10^{-4} \text{ M}$) were prepared by dissolving them in a mixture of DMSO and Tris-HCl-NaCl buffer (5:95, V/V). Then the solutions of test compounds (30 μL for each time) were dropped into the BSA solution (3 mL) and reference solution. The mixed solution was monitored by fluorescence spectrometer in the wavelength range of 300–540 nm under 28 °C. The excitation



Scheme 1. Synthetic routes of HL, **1** and **2**.

wavelength was 280 nm and the excitation/emission slit widths were all 5 nm.

2.6. Microcalorimetry experiments of HL, **1** and **2** with CT-DNA/BSA

The solutions of test compounds (1 mL, 1×10^{-4} M) and Tris-HCl/Tris-HCl-NaCl buffer solution (1 mL) were added in the bottom of the sample cell and reference cell respectively. Then 2 mL of CT-DNA (2.88×10^{-4} M) or BSA solutions (1×10^{-7} M) were added in both up of sample cell and reference cell. The sample cell and reference cell were put into microcalorimeter. After the baseline of heat flow was stable, the solutions in upper and bottom cells were mixed. And the heat flows of the reaction were recorded at 28°C . ΔH was obtained by integrating exothermic peak.

2.7. Molecular docking studies of HL, **1** and **2** with DNA/BSA

The crystal structures of DNA (PDB ID: 1XRW) and BSA (PDB ID: 3V03) were chosen from RCSB Protein Data Bank (<http://www.rcsb.org/pdb>). The ligands were removed from 1XRW.pdb and 3V03.pdb by using Discovery Studio 4.5. The crystal structures of three compounds were obtained from X-ray single crystal data, and CIF files were converted into PDB format using Mercury software. **1**, **2** and HL were added Gasteiger charges and merged non-polar hydrogen atoms by Autodock tools. Molecular docking

studies of three compounds interacting with DNA/BSA were done on Autodock 4.0 software. Genetic Algorithm was selected as 100 runs to search best conformer. For each of the docking case, the lowest energy conformation was selected as the binding mode. The visualization of the docked pose was performed using Pymol and Discovery Studio 4.5.

2.8. Antibacterial tests

Antibacterial activities of the ligand and its Co and Cu complexes were tested by the agar well diffusion method using nutrient agar media. Each test compound was dissolved in an aqueous solution of DMSO as the co-solvent with a concentration of $200 \mu\text{g}\cdot\text{mL}^{-1}$. Two species of pathogenic bacteria, *Staphylococcus aureus* (*S. aureus*) and *Bacillus subtilis* (*B. subtilis*) were used to screen the antibacterial activities of compounds. Pathogenic bacterial strains were incubated in sterile nutrient broth at 37°C for 24 h. Per dish contains 10 mL nutrient agar and 2 mL inoculums of bacterial strain ($10^6 \text{ cfu}\cdot\text{mL}^{-1}$). The Oxford cups were placed in a solidified medium. 250 μL of each test compound solution was poured in the respective cups and the plates including control group were incubated 16–18 h at 37°C . The experiment was performed in triplicate under strict aseptic conditions and the antibacterial activity of each compound was expressed in terms of the

mean diameter of zone of inhibition (mm) produced by the respective compound.

2.9. Cellular uptake studies using ICP-MS

Overnight cultured *S. aureus* and *Bacillus subtilis* (10^6 cfu·mL⁻¹) were incubated with either **1** or **2** (150 µg·mL⁻¹) for 16 h at 37 °C. After incubation, the culture tubes were centrifuged for 20 min and the resulting supernatant was removed. Then the cell pellets were washed three times with PBS buffer solution (5 mL) and re-centrifuged every time. Cellular pellets were digested with 200 µL of 70% HNO₃ and then diluted to 5 mL with 3% HNO₃. The obtained samples were measured by ICP-MS to determine the cobalt/copper content.

3. Results and discussion

3.1. Structure descriptions

The molecular structures and the illustrations of bond distance of **HL**, **1** and **2** are presented in Figs. 1–3. View of hydrogen bonds of **HL**, **1** and **2** are illustrated in Figs. S1–S3. The crystallographic data for **HL**, **1** and **2** are given in Table 1. The selected bond lengths (Å) and angles (°) are displayed in Table 2. Hydrogen bond lengths (Å) and angles (°) are shown in Table S1.

HL crystallized in the monoclinic system, space group $P2_1/c$ with bond distances and angles in the expected ranges. As shown in Table 2, C8–O2 (1.223(6) Å) is a typical C=O double bond [36]. And the N2–C9 (1.275(6) Å) is shorter than the C–N single bond (1.47 Å) [37], which could be classified as a C=N double bond [38,39]. These data show that **HL** includes a keto group. The dihedral angle of the pyridine ring and benzene ring in **HL** is 72.14° which indicates that they are not in the same plane. The torsion angles of N2–N1–C8–C7 (−178.8(4)°) and N1–N2–C9–C10 (179.5(4)°) show that the N1 and N2 atoms are not in exact parallel planes. Fig. S1 is the view of hydrogen bonds in **HL** and there are two kinds of hydrogen bonds N1–H1...O2 and O1–H1A...N2 between the adjacent molecule which forms the 2D structure in **HL**.

Complex **1** and **2** crystallized in the orthorhombic system, space group $Pbca$ and monoclinic system, space group $P2_1/n$, respectively. As seen from Fig. 2, within the cationic unit, Co²⁺ ion was coordinated by an anionic ligand **L**, a neutral ligand **HL** and NO₃⁻ anion presenting in the complex to neutralize the charge of cation. Fig. 3 shows **2** consists of a Cu²⁺ ion, two neutral ligands and the other two NO₃⁻ anions in the complex which is different from **1**. For complexes **1** and **2**, the coordination environments of Co²⁺ and Cu²⁺ ions both contain nitrile nitrogen (N2, N5), pyridyl nitrogen (N3, N6), keto oxygen (O2, O4) atoms, which occupy the apical positions of the polyhedron to form a distorted octahedral geometry.

In complex **1**, the bond length of C8–O2 (1.303(5) Å) is closed to that of C8–N1 (1.314(6) Å), it could be deduced that there exists an electron conjugated effect among C8–O2–N1 which causes the loss of a proton. Fig. S2 and Table S1 show **1** has four hydrogen bonds between ligand and NO₃⁻ to form a scissors configuration. As shown in Fig. S3 and Table S1, **2** has seven hydrogen bonds between ligand and NO₃⁻ forming a 2D structure. As far as the bond lengths of Cu complex are concerned, it is worth highlighting that the Cu1–O2 (2.183(2) Å) and Cu1–O4 (2.360(2) Å) are longer than Co1–O2 (1.904(3) Å) and Co1–O4 (1.911(3) Å) (Table 2), as a result of tetragonal elongation. Similar variation has already been observed in other literature [40,41]. The presence of tetragonal distortion leads to the conformation change of the octahedral geometry of the complexes. And the difference in the configuration moves the bonding sites of the complex away or towards the DNA. Therefore, the tetragonal distortion could influence the interactions of complex with DNA [42].

3.2. Thermal stabilities

The thermal stabilities of **HL**, **1** and **2** were studied at heating rates of 5, 10 and 15 °C·min⁻¹ in the temperature range from room temperature to 800 °C. The TG curves of **HL**, **1** and **2** at the heating rate of 5 °C·min⁻¹ are plotted in Fig. 4 and DTG curves at three heating rates are shown in Figs. S4–S6, separately. According to Fig. 4 and Fig. S4, the thermal decomposition of **HL** characterized by one stage. **HL** loses 73.62% of its mass at 199.73–420.17 °C, which is assigned to the bond breaking of C9–C10 (calcd. 71.00%). The loss group for **HL** in thermal decomposition processes are illustrated in Fig. S7. As seen from Fig. 4 and Fig. S5, complex **1** undergoes three stage of decomposition. The first decomposition stage of **1** at 221.46–285.07 °C with the weight loss of 11.37% resulting from the loss of NO₃⁻ (calcd. 10.16%). In the second stage, the weight loss is 22.61% at 285.07–463.69 °C. TG curve shows a weight loss of 56.74% in the temperature range of 463.69–800 °C at third stage. For complex **2**, one significant weight loss peak is observed from Fig. 4 and Fig. S6. It occurs with the weight loss of 19.83% at 181.61–252.90 °C corresponding to the loss of two NO₃⁻ (calcd. 17.09%). Further, **2** undergoes few hardly distinguishable stages and did not completely decomposed until 800 °C.

The kinetic parameters of main decomposition process, such as pre-exponential factor (A) and apparent activation energy (E_a) of three compounds were calculated by Kissinger (1) and Ozawa (2) equations [43]:

$$\ln\left(\frac{\beta}{T_p^2}\right) = \ln\left(\frac{AR}{E_a}\right) - \frac{E_a}{RT_p} \quad (\text{Kissinger}) \quad (1)$$

$$\lg\beta = \lg\left[\frac{AE_a}{RG(\alpha)}\right] - 2.315 - 0.4567\frac{E_a}{RT_p} \quad (\text{Ozawa}) \quad (2)$$

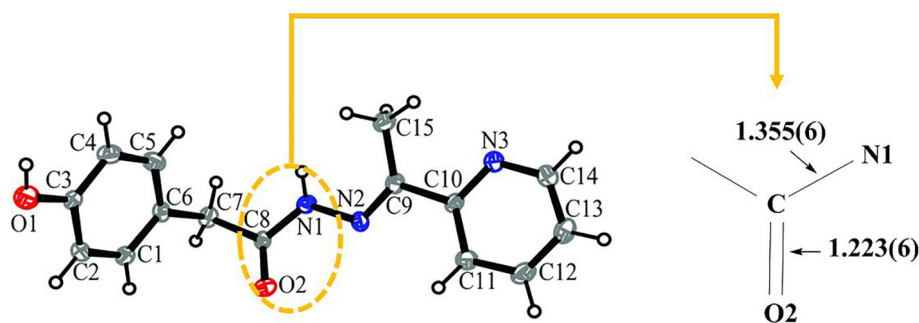


Fig. 1. Molecular structure of **HL** with 30% probability and the illustration of bond distance.

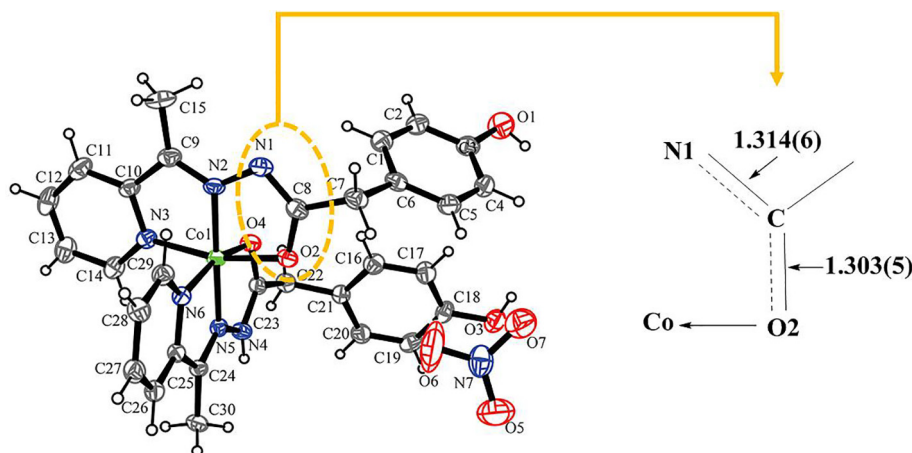


Fig. 2. Molecular structure of **1** with 30% probability and the illustration of bond distance.

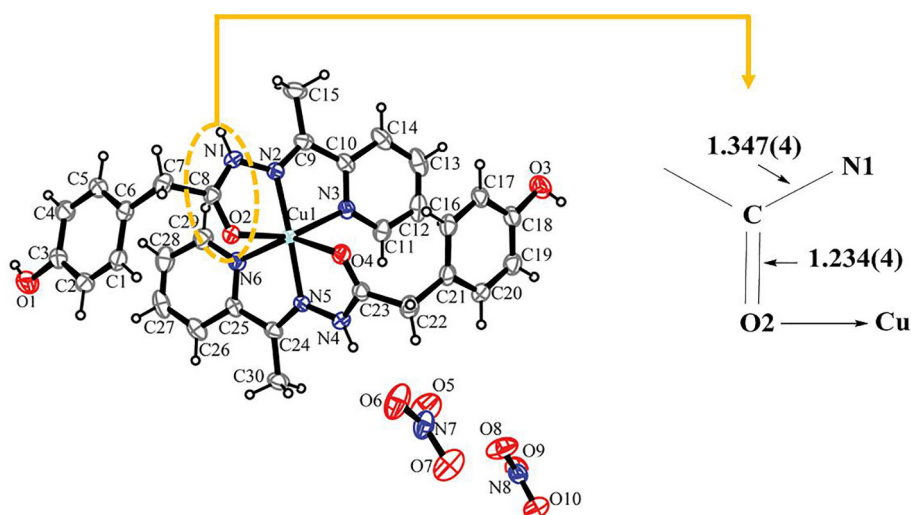


Fig. 3. Molecular structure of **2** with 30% probability and the illustration of bond distance.

Table 1
Crystallographic data for HL, **1** and **2**.

	HL	1	2
CCDC number	1474071	1524772	1475317
formula	C ₁₅ H ₁₅ N ₅ O ₂	[Co(HL)NO ₃]	[Cu(HL) ₂] (NO ₃) ₂
formula weight	269.30	658.53	726.16
crystal system	monoclinic	orthorhombic	monoclinic
space group	P2 ₁ /c	Pbca	P2 ₁ /n
a (Å)	9.468(5)	13.077(2)	1.3813(2)
b (Å)	16.836(9)	18.739(3)	1.2432(2)
c (Å)	8.776(5)	23.709(4)	1.9122(3)
α (°)	90.00	90.00	90.00
β (°)	99.669(10)	90.00	102.779(3)
γ (°)	90.00	90.00	90.00
V (Å ³)	1379.1(13)	5809.7(17)	3202.4(9)
Z	4	8	4
D _c (g·cm ⁻³)	1.297	1.510	1.506
F(0 0 0)	568	2744	1500
θ Range	2.18–25.100	2.08–25.10	1.66–25.10
T (K)	296(2)	296(2)	296(2)
final R indices (I > 2σ)	R1 = 0.1124	R1 = 0.11455	R1 = 0.0445
(I)	wR2 = 0.3914	wR2 = 0.1296	wR2 = 0.1201

where T_p is the maximum temperature of endothermic peak in the fastest decomposition stage, R the gas constant, β the heating rate, and $G(\alpha)$ the integral mechanism function. The calculated results

are listed in Table 3. It can be seen that the results calculated from the two methods are consistent and the E_a values follow the order: **2** > **1** > HL. Therefore, the decomposition of complex **2** requires more energy. And **2** displays the most excellent thermal stability among three compounds which may be related to its maximum number of hydrogen bonds [44].

3.3. Interaction of the compounds with CT-DNA

The binding behavior of the small molecule with CT-DNA was often investigated by UV–Vis absorption spectra. Generally, the changes in absorption spectra are closely related to DNA-binding mode. The absorption spectra of HL, **1** and **2** interacting with CT-DNA are given in Fig. S8, Fig. 5 and Fig. 6, respectively. The intrinsic binding constants K_{ib} of HL, **1** and **2** were calculated under the following equation (3) [45]:

$$\frac{[DNA]}{\varepsilon_a - \varepsilon_f} = \frac{[DNA]}{\varepsilon_b - \varepsilon_f} + \frac{1}{K_{ib}(\varepsilon_b - \varepsilon_f)} \quad (3)$$

where [DNA] represents the concentration of CT-DNA, ε_a the apparent extinction coefficient of the compound in the presence of CT-DNA, ε_b the molar extinction coefficient for the free compound and ε_f the molar extinction coefficient for compound fully binding with CT-DNA. The insets in Fig. S8, Fig. 5 and Fig. 6 show the plots

Table 2
Selected bond lengths (Å) and angles (°) for **HL**, **1** and **2**.

compound	bond length	bond angle	torsion angle
HL	O1-C3 1.362(6)	O1-C3-C4 123.2(4)	N2-N1-C8-O2 2.8(7)
	O2-C8 1.223(6)	O2-C8-N1 124.2(4)	N2-N1-C8-C7 -178.8(4)
	N1-C8 1.355(6)	C8-N1-N2 118.5(4)	N2-C9-C10-N3 173.0(5)
	N1-N2 1.398(5)	N2-C9-C15 126.8(4)	N1-N2-C9-C10 179.5(4)
	N2-C9 1.275(6)	C14-N3-C10 117.5(5)	C8-N1-N2-C9 -158.0(4)
1	Co1-N2 1.854(4)	N2-Co1-O2 82.17(16)	Co1-N2-N1-C8 0.6(5)
	Co1-N3 1.923(4)	N2-Co1-N3 82.69(18)	O2-Co1-N2-N1 -0.1(3)
	Co1-N6 1.947(4)	N5-Co1-O4 82.17(14)	N5-Co1-O4-C23 -2.0(3)
	Co1-N5 1.853(3)	N5-Co1-N6 81.98(15)	Co1-N5-N4-C23 2.4(4)
	Co1-O2 1.904(3)	N5-Co1-N2 179.23(18)	N2-Co1-O2-C8 -0.5(3)
	Co1-O4 1.911(3)	O2-Co1-N3 164.85(15)	N2-N1-C8-C7 175.7(4)
	C8-O2 1.306(5)	O2-Co1-O4 88.65(13)	N3-Co1-N2-N1 -179.9(3)
	C8-N1 1.314(6)	N5-Co1-N3 97.96(16)	N5-Co1-N6-C25 -1.0(3)
	C9-N2 1.295(6)	O4-Co1-N6 164.08(14)	O4-Co1-N5-C24 -179.5(4)
	Cu1-N2 1.937(3)	N2-Cu1-O2 76.75(10)	N2-Cu1-O2-C8 13.4(2)
	Cu1-N3 2.047(3)	N3-Cu1-N2 79.50(11)	N5-Cu1-O4-C23 22.5(2)
2	Cu1-O2 2.183(2)	N5-Cu1-O4 72.97(10)	N3-Cu1-N2-C9 0.0(3)
	Cu1-N5 1.962(3)	N5-Cu1-N6 77.08(11)	N6-Cu1-N5-C24 -8.0(2)
	Cu1-N6 2.168(3)	N2-Cu1-N5 176.46(11)	C8-N1-N2-Cu1 12.6(3)
	Cu1-O4 2.360(2)	O2-Cu1-N3 152.39(10)	C23-N4-N5-Cu1 18.2(3)
	C8-O2 1.234(4)	O2-Cu1-O4 87.11(8)	N5-Cu1-N3-C14 0.0(3)
	C8-N1 1.347(4)	N5-Cu1-N3 103.87(11)	N5-Cu1-N3-C10 -176.9(2)
	C9-N2 1.285(4)	N6-Cu1-O4 146.10(10)	N2-Cu1-N6-C29 -3.5(3)

of $[DNA]/(\epsilon_a - \epsilon_f)$ versus $[DNA]$. The binding constants K_{ib} , calculated by the ratio of slope to the intercept are listed in Table 4.

As observed in Fig. S8, the absorption spectra band at 283 nm showed hypochromism and a slight red shift from 283 to 285 nm with the addition of CT-DNA into **HL**. It indicated that the empty π^* orbital of **HL** couples with a π orbital of CT-DNA and the $\pi \rightarrow \pi^*$ transition energies were decreased [46]. For **1**, the band at 263 nm (Fig. 5) is probably due to the intra-ligand $\pi \rightarrow \pi^*$ transitions of **HL** and the band at 358 nm is attributable to the ligand-to-metal charge transfer (LMCT) transitions [47]. With the addition of CT-DNA into **1**, the absorption spectra band at 263 and 358 nm show hypochromism and a slight red shift of 1 nm. Fig. 6 is similar with Fig. 5, the band at 276 nm is assigned to $\pi \rightarrow \pi^*$ transitions of **HL** and 343 nm is representing the LMCT. Obvious hypochromism were also observed at 276 and 343 nm and a slight red shift was also observed from 276 nm to 284 nm. The intrinsic binding constants K_{ib} of **HL**, **1** and **2** are 2.56×10^5 , 1.71×10^8 and $1.76 \times 10^6 \text{ M}^{-1}$ and the values of two complexes are all higher than that of classical intercalator like EB ($K_{ib} = 3.3 \times 10^5 \text{ M}^{-1}$) [48]. The spectral characteristic of hypochromism and K_{ib} values

obtained for **1** and **2** suggested that complexes **1** and **2** are strongly bound to CT-DNA by intercalation mode [49].

3.4. Interaction of the compounds with BSA

Serum albumins (BSA) has been used in this experiment due to its low cost, wide availability and structural similarity to human serum albumins. Small molecules binding to BSA can be measured by fluorescence spectra. Fig. S9, Fig. 7 and Fig. 8 show the effects of test compounds on the fluorescence intensities of BSA. It can be seen that BSA emits a strong fluorescence peak at 340 nm when the exciting wavelength is 280 nm. And continuous addition of compounds into BSA solution quenched the endogenous fluorescence of BSA which indicates that **HL**, **1**, **2** could bind to the BSA and result in microenvironment change around the tryptophan of the BSA [50,51].

To further clarify the quenching process, fluorescence quenching data were analysis by Stern-Volmer equation (4) with the hypothesis that dynamic process occurred [52,53]:

$$F_0/F = 1 + K_q \tau_0 [Q] = 1 + K_{sv} [Q] \quad (4)$$

where F_0 , F represent the fluorescence intensities in the absence and presence of quencher, respectively, K_{sv} the Stern-Volmer quenching constant, $[Q]$ the quencher concentration, K_q the bimolecular quenching constant, τ_0 the average lifetime of protein in the absence of quencher, and its value is 10^{-8} s [54]. K_{sv} and K_q values were obtained from the plots of F_0/F versus $[Q]$ (as insets in Fig. S9, Fig. 7 and Fig. 8) and shown in Table S2.

The K_q values corresponding to **HL**, **1** and **2** go beyond the limit of dynamic quenching rate constant $2 \times 10^{10} \text{ M}^{-1} \cdot \text{s}^{-1}$ [55]. Thus, the preceding assumption is invalid and the quenching processes of three compounds interacting with BSA are static quenching. It can be described by Scatchard equation (5) [56]:

$$\lg[(F_0 - F)/F] = \lg K_A + n \lg [Q] \quad (5)$$

where K_A and n are binding constant and the number of binding sites, respectively. Binding constants obtained from the plots of $\lg[(F_0 - F)/F]$ versus $\lg [Q]$ (Fig. S10) and listed in Table 5.

In Table 5, the values of K_A follow sequence **1**>**2**>**HL** suggesting that complexes have stronger protein-binding abilities than **HL**.

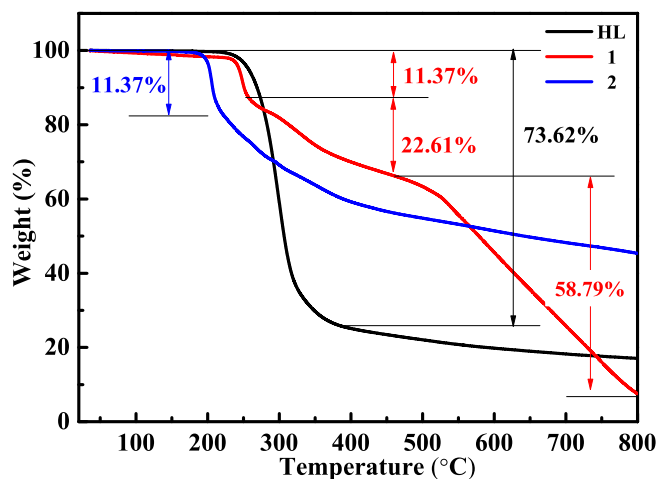


Fig. 4. TG curves of **HL**, **1** and **2** ($\beta = 5 \text{ }^\circ\text{C} \cdot \text{min}^{-1}$).

Table 3
Kinetic parameters of thermal decomposition processes of **HL**, **1** and **2**.

compound	β ($^{\circ}\text{C}\cdot\text{min}^{-1}$)	T_p ($^{\circ}\text{C}$)	Kissinger			Ozawa	
			E_a ($\text{kJ}\cdot\text{mol}^{-1}$)	$\lg A$	r	E_a ($\text{kJ}\cdot\text{mol}^{-1}$)	r
HL	5	300.21	155.7	11.85	-0.9991	157.2	-0.9992
	10	312.47					
	15	318.82					
1	5	249.81	257.1	23.68	-0.9883	252.8	-0.9891
	10	254.57					
	15	259.38					
2	5	206.35	450.5	47.43	-0.9442	636.0	-0.9460
	10	207.83					
	15	210.70					

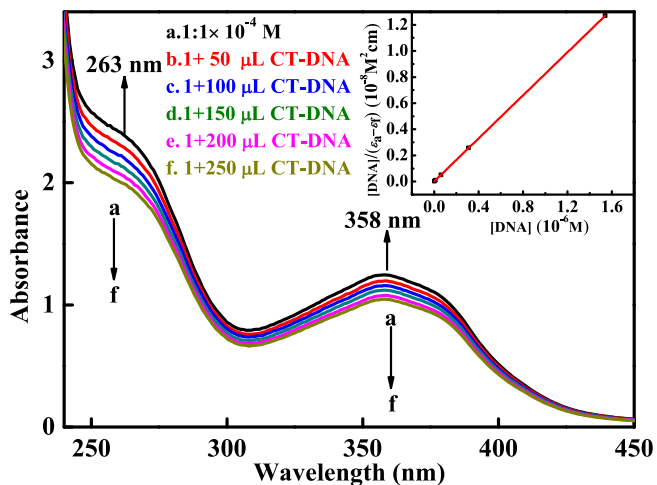


Fig. 5. UV-Vis absorption spectra of CT-DNA interacting with **1** (Inset: plot of $[\text{DNA}]/(\epsilon_a-\epsilon_f)$ versus $[\text{DNA}]$).

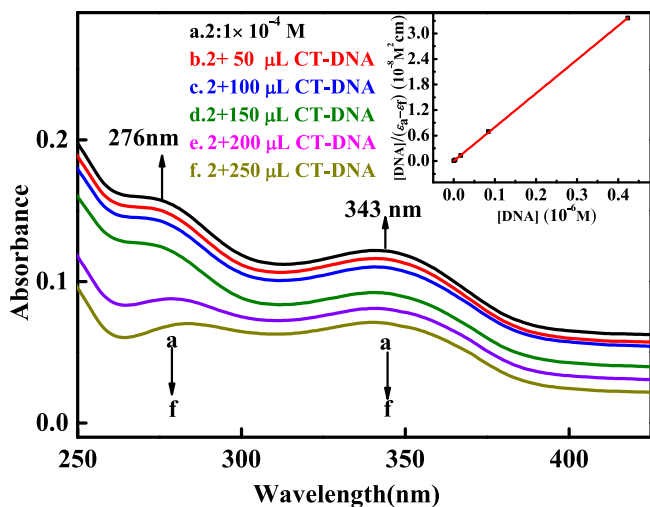


Fig. 6. UV-Vis absorption spectra of CT-DNA interacting with **2** (Inset: plot of $[\text{DNA}]/(\epsilon_a-\epsilon_f)$ versus $[\text{DNA}]$).

Moreover, the values of binding site are close to 1, showing that there exists a single binding site in BSA for **HL**, **1** and **2**. Thus, the tryptophan residues involved in the interactions might be Trp213 or Trp134 [57]. Overall, BSA can be considered as an excellent carrier to transport the entire three compounds in vivo.

Table 4
Parameters for the interactions of **HL**, **1** and **2** with CT-DNA.

compound	K_{ib} (M^{-1})	linear fitting equation	R^2
HL	2.56×10^5	$C_{\text{DNA}}/(\epsilon_a-\epsilon_f) = 1.202 \times 10^{-4} C_{\text{DNA}} - 4.69 \times 10^{-10}$	0.9911
1	1.71×10^8	$C_{\text{DNA}}/(\epsilon_a-\epsilon_f) = 8.245 \times 10^{-5} C_{\text{DNA}} + 4.81 \times 10^{-14}$	1
2	1.76×10^6	$C_{\text{DNA}}/(\epsilon_a-\epsilon_f) = 7.933 \times 10^{-5} C_{\text{DNA}} + 4.49 \times 10^{-12}$	0.9999

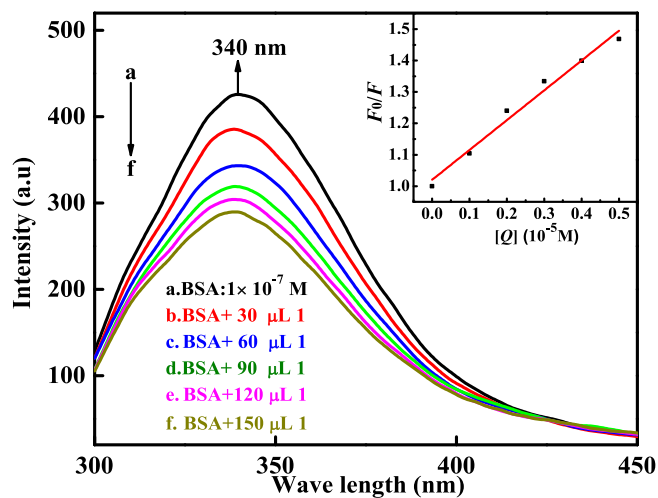


Fig. 7. Fluorescence emission spectrum of **1** interacting with BSA (Inset: plot of F_0/F versus $[Q]$).

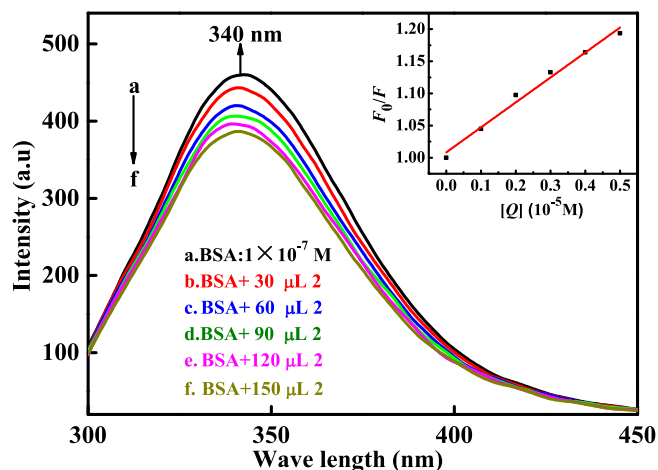


Fig. 8. Fluorescence emission spectrum of **2** interacting with BSA (Inset: plot of F_0/F versus $[Q]$).

Table 5
Parameters for the interactions of **HL**, **1** and **2** with BSA calculated by Scatchard equation.

compound	K_A (M^{-1})	n	linear fitting equation	R^2
HL	1.03×10^4	0.89	$\lg[(F_0-F)/F] = 0.89\lg[Q] + 4.01$	0.9921
1	4.20×10^4	0.93	$\lg[(F_0-F)/F] = 0.93\lg[Q] + 4.62$	0.9735
2	1.24×10^4	0.90	$\lg[(F_0-F)/F] = 0.90\lg[Q] + 4.09$	0.9840

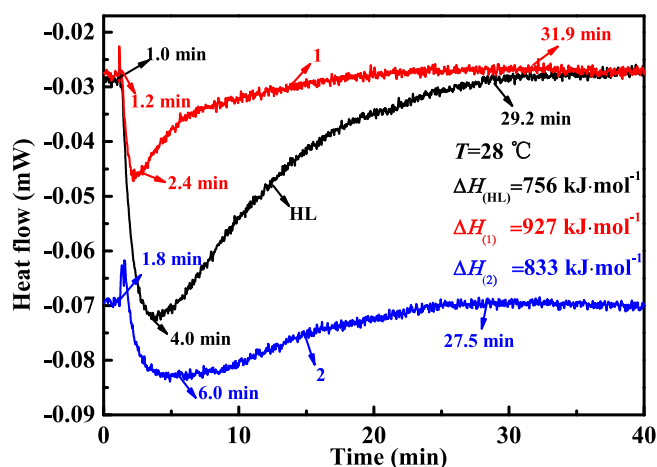


Fig. 9. Thermogenic curves of **HL**, **1** and **2** with CT-DNA.

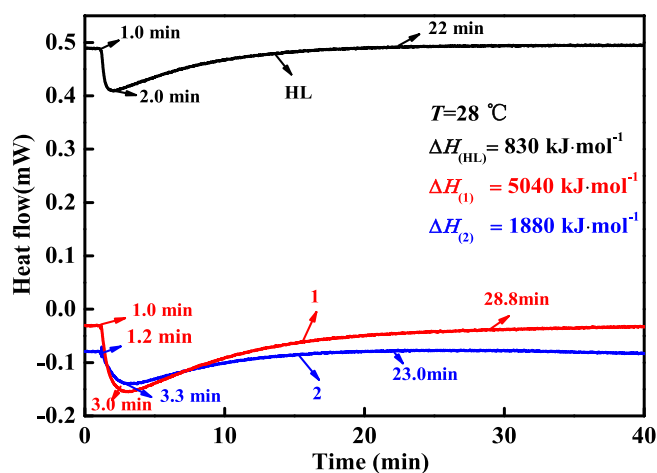


Fig. 10. Thermogenic curves of **HL**, **1** and **2** with BSA.

3.5. Microcalorimetry studies of compounds with DNA/BSA

Figs. 9 and 10 are the thermogenic curves of **HL**, **1** and **2** interacting with CT-DNA and BSA, respectively. Gibbs' free energy change (ΔG) and entropy change (ΔS) are calculated by the equations (6) and (7) [58,59]:

$$\Delta S = (\Delta H - \Delta G)/T \quad (6)$$

$$\Delta G = -RT \ln K \quad (7)$$

where ΔH is enthalpy change obtained by integrating the peak area, R the gas constant, T the experimental temperature, K the binding constant has been calculated by equation (3) and (5) as above mentioned. The corresponding parameters are listed in Table S3. As shown in Figs. 9, 10 and Table S3, the duration time of DNA/BSA interaction is within 40 min for each compound and the positive

values of ΔH suggest that the interaction between **HL**, **1**, **2** and CT-DNA/BSA are all endothermic. All the ΔG values are negative, indicating that interaction processes are spontaneous reaction and driven by entropy. Moreover, $\Delta H > 0$, $\Delta S > 0$ mean that hydrophobic forces play a major role in the binding between **HL**, **1**, **2** and CT-DNA/BSA [60,61].

3.6. Molecular docking studies of compounds with DNA/BSA

The molecular docking technique was used to identify binding locations and mechanisms of three compounds interacting with DNA/BSA. Docking studies have been performed on DNA with the sequence of d(CCTCGTCC)₂ in the presence of **HL**, **1** and **2**. The best docking perspectives of three compounds with DNA are shown in Fig. S11, Fig. 11 and Fig. 12. These docked poses show the intercalation mode of DNA with **HL**, **1** and **2** which is agreement with the spectroscopy experiment results. O2 atom and O1-H1A group of **HL** formed two hydrogen bonds with DG5 in DNA double strand. There are several hydrophobic contacts between **HL** and DG4, DG5 in DNA double strand. In the case of complex **1**, hydrogen bonding interaction was observed between N1-H4 group and phosphate oxygen atom of DC7. O1-H1A group exhibited hydrogen bonding interactions with oxygen atom of DG5. The N-H group of DG5 in another DNA strand formed hydrogen bond with O2 atom in **1**. Additionally, **1** has hydrophobic contacts with bases of DNA at DG 4, DG 5 and DT6. The O3-H3 group in complex **2** interacted with deoxyribose oxygen atoms of DG2 to form hydrogen bond. Also, N-H groups in DC4 residue displayed hydrogen bonding with O2 and O5 atoms of complex **2**. In addition, there also exist hydrophobic interactions between **2** and DA3, DC4, DG5, DC4 nucleobases.

The best docking poses of three compounds with BSA are shown in Fig. S12, Fig. 13 and Fig. 14. As can be seen, **HL** docked around Trp134 in subdomain IB, whereas complex **1** and **2** docked around Trp213 in subdomain IIA [59]. It also supports the fluorescence quenching of tryptophan in BSA in presence of **HL**, **1** and **2** which is obtained from fluorescence spectroscopy experimental results (Section 3.4). In ligand **HL**, O-H...O hydrogen bond formed between the compound and the ASP108 residue. It also involved in hydrophobic interactions with ARG196, HIS145, ARG144 and PRD110. Similarly, The O1-H1A group in complex **1** interacted with oxygen atom of GLU339 residue to form hydrogen bond. There also exists electrostatic interaction between **1** and protein residue GLU443. Several categories of hydrophobic interactions were detected between **1** and GLU293, LYS294, ARG217, VAL342, PRO446 and CYS447. The O-H group in complex **2** also interacted with oxygen atoms of GLN220 and TYR156 to form two hydrogen bonds. And the N-H group of ARG194 formed hydrogen bond with O4 atom in **2**. In addition, complex **2** exhibited electrostatic interaction with GLU291 and hydrophobic interactions with ARG217, LYS221 and LYS187.

According to the molecular docking studies results, hydroxyl group of benzene ring, benzene ring, pyridine ring, and carbonyl group of test compound are the most favorable binding site in DNA/BSA interaction. Hydrophobic force is the main force in the binding of **HL**, **1** and **2** to DNA/BSA which is consistent with the microcalorimetry experimental results.

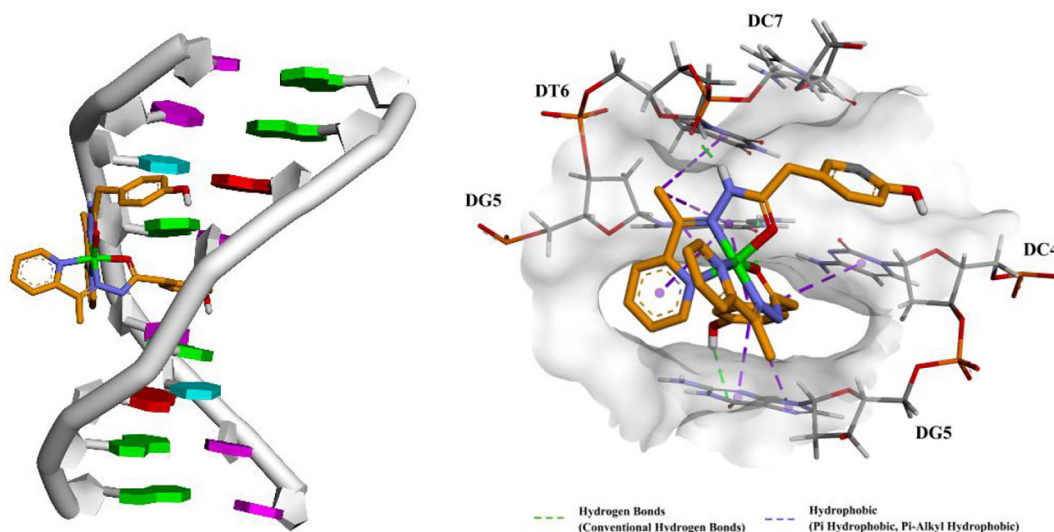


Fig. 11. Molecular docking perspective of the **1** with DNA and three-dimensional interactions generated by Discovery Studio 4.5 (right).

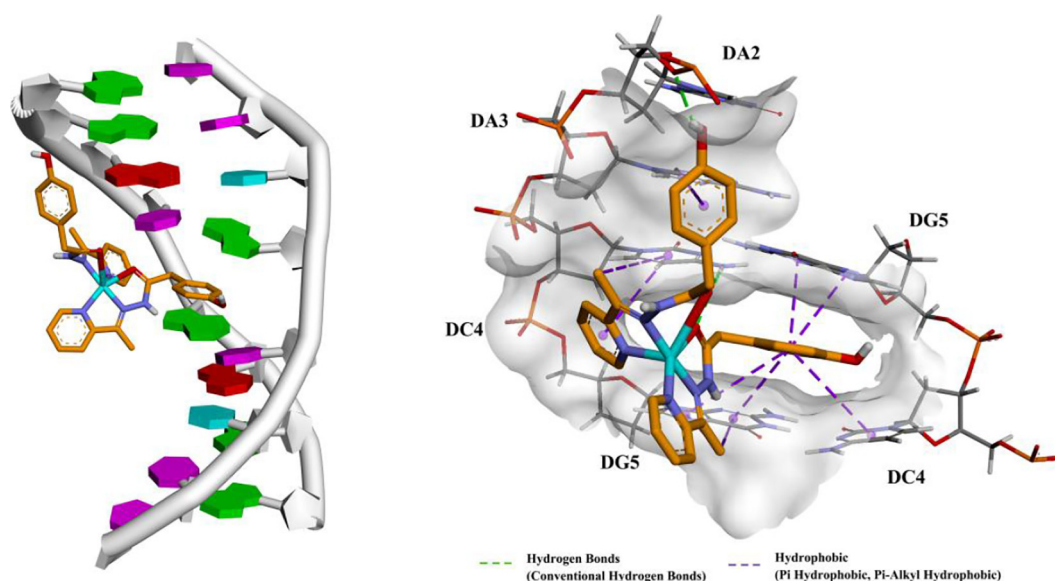


Fig. 12. Molecular docking perspective of the **2** with DNA and three-dimensional interactions generated by Discovery Studio 4.5 (right).

3.7. Antibacterial activities studies

S. aureus and *B. subtilis* are used to evaluate the antibacterial activities of **HL**, **1** and **2**. From the data presented in Table S4, it can be seen that **1** exhibits best antibacterial activity against *S. aureus* with a MIC value of $150 \mu\text{g}\cdot\text{mL}^{-1}$ while **HL** and **2** are inactive against *S. aureus* (if antimicrobial zone less than 8 mm, the compound can be judged inactive for bacteria). Also, **HL** can inhibit the growth of *B. subtilis* with a MIC value of $200 \mu\text{g}\cdot\text{mL}^{-1}$. This may be due to **1** possesses excellent binding ability with CT-DNA/BSA, which is playing an essential role in the antibacterial activity. Besides, the antibacterial ability of metal complexes could also be related to the nature of ion, geometry of complexes, steric, pharmacokinetic, hydrophilicity and lipophilicity [62].

3.8. Cellular uptake of complexes into bacterial cells

The cellular uptakes results of the complexes **1** and **2** into *S. aureus* and *B. subtilis* are displayed in Table 6. These results showed

that both Co and Cu were accumulated in *S. aureus* and *B. subtilis*. The amount of Co accumulation in *S. aureus* is bigger than that of Cu. And the cellular uptake amounts of Co and Cu in *B. subtilis* are basically the same and all lower.

4. Conclusion

A new ligand 2-acetylpyridine-4-hydroxy phenylacetyl acylhydrazide (**HL**) and its two complexes $[\text{Co}(\text{HL})\text{L}]\text{NO}_3$ (**1**) and $[\text{Cu}(\text{HL})_2](\text{NO}_3)_2$ (**2**) were synthesized. The results of single-crystal XRD showed **1** and **2** are mononuclear and belong to orthorhombic, space group *Pbca* and monoclinic, space group *P2₁/n*, respectively. Thermal stability of three compounds follow the sequence: **2**>**1**>**HL**. The interactions of **1**, **2** and **HL** with CT-DNA/BSA were studied by UV-Vis spectroscopy and fluorescence spectroscopy separately, revealing intercalation mode between compounds and CT-DNA and static quenching mechanism in BSA fluorescence quenching. The binding constants of three compounds interacting with CT-DNA/BSA both follow the order: **1**>**2**>**HL**. Microcalorime-

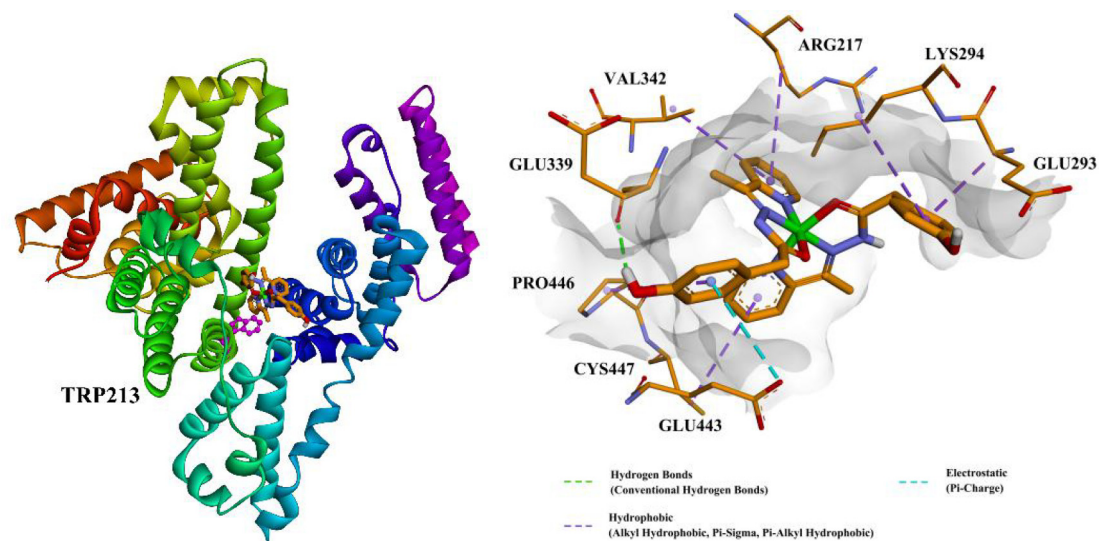


Fig. 13. Molecular docking perspective of the **1** with BSA (left) and three-dimensional interactions generated by Discovery Studio 4.5 (right).

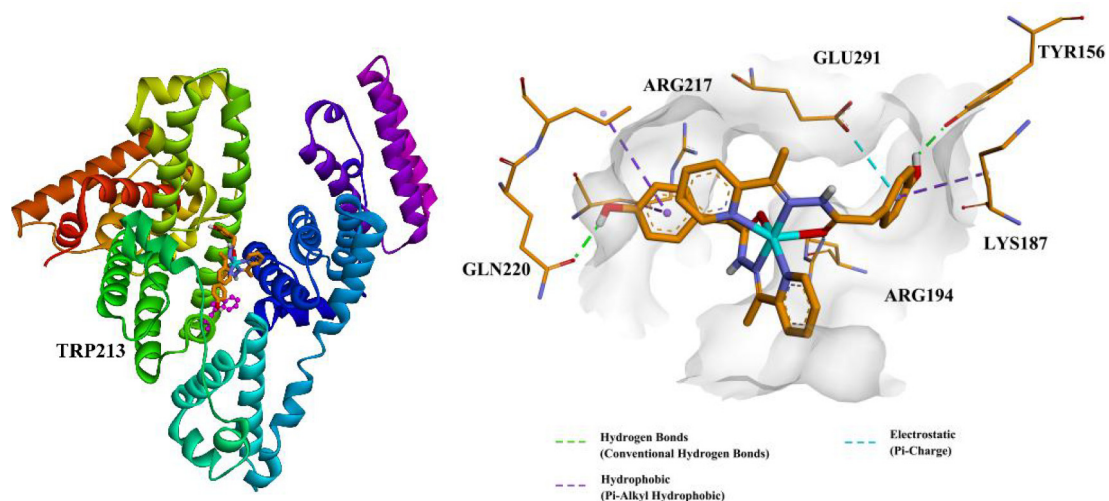


Fig. 14. Molecular docking perspective of the **2** with BSA and three-dimensional interactions generated by Discovery Studio 4.5 (right).

Table 6
Cellular uptakes of complexes **1** and **2** into *S. aureus* and *B. subtilis*.

bacteria	complex 1 Co ($\mu\text{g}/10^6$ cells)	complex 2 Cu ($\mu\text{g}/10^6$ cells)
<i>S. aureus</i>	2.59	1.19
<i>B. subtilis</i>	1.41	1.44

try results showed the interactions of three compounds with CT-DNA/BSA are endothermic processes and hydrophobic force mainly contributes in the interaction between **1**, **2**, **HL** and CT-DNA/BSA. Molecular docking results confirmed the intercalation mode between compounds and CT-DNA. And **HL** docked around Trp134 in subdomain IB, whereas complex **1** and **2** docked around Trp213 in sub-domain IIA. Hydroxyl group of benzene ring, benzene ring, pyridine ring, and carbonyl group of three compounds were main binding sites in DNA/BSA interaction. Antibacterial studies showed that **1** and **HL** can inhibit the growth of *B. subtilis* and *S. aureus* with MIC values of $150 \mu\text{g}\cdot\text{mL}^{-1}$ and $200 \mu\text{g}\cdot\text{mL}^{-1}$, respectively. The amount of Co accumulation in *S. aureus* is

$2.59 \mu\text{g}/10^6$ cells which is bigger than that of Cu, the accumulations of Co and Cu in *B. subtilis* are all lower.

CRediT authorship contribution statement

Jie Yang: Investigation, Writing - original draft. **Xiang-rong Liu:** Investigation, Writing - review & editing, Funding acquisition. **Ming-kun Yu:** Investigation. **Wen-bo Yang:** Validation. **Zai-wen Yang:** Data curation. **Shun-sheng Zhao:** Formal analysis.

Declaration of Competing Interest

The authors declare that they have no known competing financial interests or personal relationships that could have appeared to influence the work reported in this paper.

Acknowledgments

This work was supported by the National Natural Science Foundation of China (Nos. 21073139, 21373158, U1903133), Science

and Technology on Combustion and Explosion Laboratory Foundation of Shaanxi (No. 6142603010301), and Analytical Instrumentation Center of XUST.

Appendix A. Supplementary data

CCDC 1474071, 1524772, 1475317 contains the supplementary crystallographic data for **HL**, **1** and **2**. These data can be obtained free of charge via <http://www.ccdc.cam.ac.uk/conts/retrieving.html>, or from the Cambridge Crystallographic Data Centre, 12 Union Road, Cambridge CB2 1EZ, UK; fax: (+44) 1223-336-033; or e-mail: deposit@ccdc.cam.ac.uk. Supplementary data to this article can be found online at <https://doi.org/10.1016/j.poly.2020.114619>.

References

- [1] M. Sedighipour, A.H. Kianfar, M.R. Sabzalian, F. Abyar, *Spectrochim. Acta, Part A* 198 (2018) 38–50, <https://doi.org/10.1016/j.saa.2018.02.050>.
- [2] Y. Burgos-Lopez, J.D. Plá, L.M. Balsa, I.E. León, G.A. Echeverría, O.E. Piro, J. García-Tojal, R. Pis-Diez, A.C. González-Baró, B.S. Parajón-Costa, *Inorg. Chim. Acta* 487 (2019) 31–40, <https://doi.org/10.1016/j.ica.2018.11.039>.
- [3] D. Saini, M. Gupta, *Asian J. Pharm. Pharmacol.* 4 (2018) 116–122. doi: 10.31024/ajpp.2018.4.2.4.
- [4] N.G. Kandile, M.I. Mohamed, H.M. Ismael, *J. Enzyme Inhib. Med. Chem.* 32 (2017) 119–129, <https://doi.org/10.1080/14756366.2016.1238365>.
- [5] J.V. Cerqueira, C.S. Meira, E.S. Santos, L.S.A. França, J.F. Vasconcelos, C.K.V. Nonaka, T.L. Melo, J.M.S. Filho, D.R.M. Moreira, M.B.P. Soares, *Int. Immunopharmacol.* 75 (2019) 285–292, <https://doi.org/10.1016/j.intimp.2019.105735>.
- [6] H.A. El-Sayed, A.H. Moustafa, M.A. El-Moneim, H.M. Awad, A. Esmat, *J. Pharm. Appl. Chem.* 4 (2018) 125–131. doi: 10.18576/jpac/040207.
- [7] M.A. Abdelrahmana, I. Salamab, M.S. Gomaab, M.M. Elaisserc, M.M. Abdel-Aziz, D.H. Soliman, *Eur. J. Med. Chem.* 138 (2017) 698–714, <https://doi.org/10.1016/j.ejmech.2017.07.004>.
- [8] P. Kumar, K. Kadyan, M. Duhan, J. Sindhu, V. Singh, B.S. Saharan, *Chem. Cent. J.* 11 (2017) 115–128, <https://doi.org/10.1186/s13065-017-0344-7>.
- [9] P. Nagender, R.N. Kumar, G.M. Reddy, D.K. Swaroop, Y. Poornachandra, C.G. Kumar, B. Narsaiah, *Bioorg. Med. Chem. Lett.* 26 (2016) 4427–4432, <https://doi.org/10.1016/j.bmcl.2016.08.006>.
- [10] H. Elshafly, T.R. Todorovic, M. Nikolic, A. Lolic, A. Višnjevac, S. Hagenow, J.M. Padrón, A.T. García-Sosa, I.S. Djordjević, S. Grubišić, H. Stark, N.R. Filipović, *Front. Chem.* 6 (2018) 247–265. doi: 10.3389/fchem.2018.00247.
- [11] P. Bera, P. Brandão, G. Mondal, H. Jana, A. Jana, A. Santra, P. Bera, *Polyhedron* 134 (2017) 230–237, <https://doi.org/10.1016/j.poly.2017.06.024>.
- [12] A.E. Dissouky, O.A. Fulaij, M.K. Awad, S. Rizk, *J. Coord. Chem.* 62 (2010) 330–345, <https://doi.org/10.1080/00958970903366959>.
- [13] A. Datta, P.H. Liu, J.H. Huang, E. Garribba, M. Turnbull, B. Machura, C.L. Hsu, W.T. Chang, A. Pevecg, *Polyhedron* 44 (2012) 77–87, <https://doi.org/10.1016/j.poly.2012.06.027>.
- [14] I. Kostova, L. Saso, *Curr. Med. Chem.* 20 (2013) 4609–4632, <https://doi.org/10.2174/09298673113209990149>.
- [15] L.D. Popov, A.N. Morozov, I.N. Shcherbakov, Y.P. Tupolova, V.V. Lukov, V.A. Kogan, *Russ. Chem. Rev.* 78 (2009) 643–658, <https://doi.org/10.1002/chin.201002231>.
- [16] L. Tabrizi, P. McArdle, A. Erxleben, H. Chiniforoshan, *Eur. J. Med. Chem.* 103 (2015) 516–529, <https://doi.org/10.1016/j.ejmech.2015.09.018>.
- [17] D. Anastasiadou, G. Psomas, S. Kalogiannis, G. Geromichalos, A.G. Hatzidimitriou, P. Aslanidis, *J. Inorg. Biochem.* 198 (2019), <https://doi.org/10.1016/j.jinorgbio.2019.110750>.
- [18] Y. Zhang, L. Zhang, L. Liu, J. Guo, D. Wu, G. Xu, X. Wang, D. Jia, *Inorg. Chim. Acta* 363, (2010) 289–293. doi: 10.1016/j.ica.2009.08.017.
- [19] S. Anbu, A. Paul, R. Ravishankaran, M.F.C.G.D. Silva, A.A. Karande, A.J.L. Pombeiro, *Inorg. Chim. Acta* 423 (2014) 183–193, <https://doi.org/10.1016/j.ica.2014.07.016>.
- [20] P. Sureshbabu, M. Mondal, N. Sakthivel, S. Sabiah, *J. Coord. Chem.* 71 (2018) 3615–3638, <https://doi.org/10.1080/00958972.2018.1527029>.
- [21] R. Bhaskar, N. Salunkhe, A. Yaul, A. Aswar, *Spectrochim. Acta, Part A* 151 (2015) 621–627, <https://doi.org/10.1016/j.saa.2015.06.121>.
- [22] K. Mahajan, M. Swami, R.V. Singh, *Russ. J. Chem.* 35 (2009) 179–185, <https://doi.org/10.1134/S1070328409030038>.
- [23] M. Mohamadi, A. Rezaei, S.Y. Ebrahimipour, S.K. Falahati-pour, F. Mohamadizadeh, M. Bemani, M.R. Hajizadeh, M.R. Mirzaei, A. Khoshdel, M. Mahmoodi, *Chem. Select.* 4 (2019) 13932–13939, <https://doi.org/10.1002/slct.201904120>.
- [24] K. Sakthikumar, R.V. Solomon, J.D. Raja, *RSC Adv.* 9 (2019) 14220–14241, <https://doi.org/10.1039/C8RA09218D>.
- [25] M.A. Neelakantan, M. Sundaram, M.S. Nair, *Spectrochim. Acta, Part A* 79 (2011) 1693–1703, <https://doi.org/10.1016/j.saa.2011.05.037>.
- [26] N. Nanjundan, P. Selvakumar, R. Narayanasamy, R.A. Haque, K. Velmurugan, R. Nandhakumar, T. Silambarasan, R. Dhandapani, *J. Photochem. Photobiol. B* 141 (2014) 176–185, <https://doi.org/10.1016/j.jphotobiol.2014.10.009>.
- [27] J. Zhao, W. Li, R. Ma, S. Chen, S. Ren, T. Jiang, *Int. J. Mol. Sci.* 14 (2013) 16851–16865, <https://doi.org/10.3390/ijms140816851>.
- [28] R. Bera, B.K. Sahoo, K.S. Ghosh, S. Dasgupta, *Int. J. Biol. Macromol.* 42 (2008) 14–21, <https://doi.org/10.1016/j.ijbiomac.2007.08.010>.
- [29] T. Kondori, N. Akbarzadeh-T, K. Abdi, M. Dušek, V. Eigner, *J. Biomol. Struct. Dyn.* 38 (2020) 236–247, <https://doi.org/10.1080/07391102.2019.1570867>.
- [30] N. Balakrishnan, J. Haribabu, D. A. Krishnan, S. Swaminathan, D. Mahendiran, N. S. P. Bhuvanesh, R. Karvembu, *Polyhedron*. 170 (2019) 188–201. doi: 10.1016/j.poly.2019.05.039
- [31] M.T. Larsen, O.A. Mandrup, K.K. Schelde, Y. Luo, K.D. Sørensen, F.D. Hansen, J. Cameron, M. Stougaard, T. Steiniche, K.A. Howard, *J. Controlled Release* (2020), <https://doi.org/10.1016/j.jconrel.2020.03.004>.
- [32] H. Hyun, J. Park, K. Willis, J.E. Park, L.T. Lyle, W. Lee, Y. Yeo, *Biomaterials* 180 (2018) 206–224, <https://doi.org/10.1016/j.biomaterials.2018.07.024>.
- [33] J. Flarakos, K. L. Morand, P. Vouros, *Anal. Chem.* 77 (2005) 1345–1353. doi: 10.1021/ac048685z.
- [34] L.F. Chin, S.M. Kong, H.L. Seng, K.S. Khoo, R. Vikneswaran, S.G. Teoh, M. Ahmad, S.B.A. Khoo, M.J. Maah, C.H. Ng, *J. Inorg. Biochem.* 105 (2011) 339–347, <https://doi.org/10.1016/j.jinorgbio.2010.11.018>.
- [35] D.S. Raja, N.S.P. Bhuvanesh, K. Natarajan, *Dalton Trans.* 41 (2012) 4365–4377, <https://doi.org/10.1039/C2DT12274J>.
- [36] M. Mehmood, I. Din, M.N. Tahir, I. Haq, S.S. Zahra, *Inorg. Chim. Acta* 486 (2019) 387–394, <https://doi.org/10.1016/j.ica.2018.10.009>.
- [37] P. Singh, D.P. Singh, V.P. Singh, *Polyhedron* 81 (2014) 56–65, <https://doi.org/10.1016/j.poly.2014.05.066>.
- [38] G. Giorgi, F. Ponticelli, L. Savini, L. Chiasserini, C. Pellerano, *J. Chem. Soc., Perkin Trans. 2* (11) (2000) 2259–2264, <https://doi.org/10.1039/B004448M>.
- [39] D.P. Singh, D.S. Raghuvanshi, K.N. Singh, V.P. Singh, *J. Mol. Catal. A: Chem.* 379 (2013) 21–29, <https://doi.org/10.1016/j.molcata.2013.07.011>.
- [40] A. Sousa-Pedrares, N. Camiña, J. Romero, M.L. Durán, J.A. García-Vázquez, A. Sousa, *Polyhedron*. 27 (2008) 3391–3397, <https://doi.org/10.1016/j.poly.2008.08.011>.
- [41] J. Pushparaju, N.R. Sangeetha, S. Pal, *Transition Met. Chem.* 25 (2000) 529–533, <https://doi.org/10.1023/A:1007049924860>.
- [42] C.H. Ng, K.C. Kong, S.T. Von, P. Balraj, P. Jensen, E. Thirthagiri, H. Hamadae, M. Chikira, *Dalton Trans.* 4 (2008) 447–454, <https://doi.org/10.1039/B709269E>.
- [43] R.Z. Hu, S.L. Gao, F.Q. Zhao, Q.Z. Shi, T.L. Zhang, J.J. Zhang, *Thermal Analysis Kinetics*, second ed., Science Press, Beijing, (2008) 79–120. (in Chinese).
- [44] M. Manimohan, S. Pugalmani, M.A. Sithique, *Int. J. Biol. Macromol.* 136 (2019) 738–754, <https://doi.org/10.1016/j.ijbiomac.2019.06.115>.
- [45] S. Manna, E. Zangrando, H. Puschmann, S. C. Manna, *Polyhedron*. 162 (2019) 285–292. doi: 10.1016/j.poly.2019.01.057.
- [46] J. Eberhard, I. Stoll, R. Brockhinke, B. Neumann, H.G. Stammler, A. Riefer, E. Rauls, W.G. Schmidt, J. Mattay, *CrystEngComm*. 15 (2013) 4225–4248, <https://doi.org/10.1039/C2CE26388B>.
- [47] T.M.A. Ismail, *J. Coord. Chem.* 58 (2005) 141–151, <https://doi.org/10.1080/0095897042000274733>.
- [48] L.Z. Li, Q. Guo, J.F. Dong, T. Xu, J.H. Li, *J. Photochem. Photobiol., B* 125 (2013) 56–62, <https://doi.org/10.1016/j.jphotobiol.2013.05.007>.
- [49] Z. Asadi, E. Haddadi, M. Sedaghat, *J. Photochem. Photobiol., A* 337 (2017) 140–150, <https://doi.org/10.1016/j.jphotochem.2017.01.022>.
- [50] Y.L. Zhang, X. Zhang, X.C. Fei, S.L. Wang, H.W. Gao, *J. Hazard. Mater.* 182 (2010) 877–885, <https://doi.org/10.1016/j.jhazmat.2010.06.131>.
- [51] E.A. Popova, A.V. Protas, A.V. Mukhametshina, G.K. Ovsepyan, R.V. Suezov, A.V. Eremin, E.I. Stepchenkova, E.R. Tarakhovskaya, A.V. Fonin, G.L. Starova, O.V. Mikolaichuk, Y.B. Porozov, M.A. Gureev, R.E. Trifonov, *Polyhedron* 158 (2019) 36–46, <https://doi.org/10.1016/j.poly.2018.10.038>.
- [52] N. Akbay, Z. Seferoglu, E. Gök, *J. Fluoresc.* 19 (2009) 1045–1051, <https://doi.org/10.1007/s10895-009-0504-9>.
- [53] M. Mishra, K. Tiwari, S. Shukla, R. Mishra, V.P. Singh, *Spectrochim. Acta, Part A* 132 (2014) 452–464, <https://doi.org/10.1016/j.saa.2014.05.007>.
- [54] J. Wang, L.J. Liu, B. Liu, Y. Guo, Y.Y. Zhang, R. Xu, S.X. Wang, X.D. Zhang, *Spectrochim. Acta, Part A* 75 (2009) 366–374, <https://doi.org/10.1016/j.saa.2009.10.042>.
- [55] G. Mandal, M. Bardhan, T. Ganguly, *Colloids Surf., B* 81 (2010) 178–184, <https://doi.org/10.1016/j.colsurfb.2010.07.002>.
- [56] G.W. Zhang, N. Zhao, X. Hu, J. Tian, *Spectrochim. Acta, Part A* 76 (2010) 410–417, <https://doi.org/10.1016/j.saa.2010.04.009>.
- [57] A.V. Protas, E.A. Popova, O.V. Mikolaichuk, Y.B. Porozov, A.R. Mehtiev, I. Ott, G. V. Alekseev, N.A. Kasyanenko, R.E. Trifonov, *Inorg. Chim. Acta*. 473 (2018) 133–144, <https://doi.org/10.1016/j.ica.2017.12.040>.
- [58] K. Karami, M. Alinaghi, Z. Amirghofran, J. Lipkowski, *Inorg. Chim. Acta*. 41 (2018) 797–807, <https://doi.org/10.1016/j.ica.2017.02.027>.
- [59] O.A. Chaves, V.A. da Silva, C.M.R. Sant'Anna, A.B.B. Ferreira, T.A.N. Ribeiro, M.G. de Carvalho, D. Cesarin-Sobrinho, J.C. Netto-Ferreira, *J. Mol. Struct.* 1128 (2017) 606–611, <https://doi.org/10.1016/j.molstruc.2016.09.036>.
- [60] S. Yasmeen, Riyazuddeen, *Thermochim. Acta* 655 (2017) 76–86, <https://doi.org/10.1016/j.tca.2017.06.010>.
- [61] L. Zarei, Z. Asadi, M. Dusek, V. Eigner, *J. Photochem. Photobiol. A* 374 (2019) 145–160, <https://doi.org/10.1016/j.jphotochem.2019.02.001>.
- [62] K.A. Kumar, K.L. Reddy, *Supramol. Chem.* 22 (2010) 629–643, <https://doi.org/10.1080/10610278.2010.510194>.